Color Change Measurements of Gravitational Microlensing Events by Using the Difference Image Analysis Method

Cheongho Han,

Seong-Hong Park

Department of Astronomy & Space Science,
Chungbuk National University, Chongju, Korea 361-763
cheongho,parksh@astronomy.chungbuk.ac.kr

ABSTRACT

Detecting color changes of a gravitational microlensing event induced by the limb-darkened extended source effect is important to obtain useful information both about the lens and source star. However, precise measurements of the color changes are hampered by the blending effect, which also causes color changes of the event. In this paper, we show that although the color change measured from the subtracted image by using the recently developed photometric method of the "difference image analysis" (DIA) differs from the color change measured by using the conventional PSF method, the color-change curve constructed by using the DIA method (DIA color-change curve) enables one to obtain the same information about the lens and source star, but with significantly reduced uncertainties due to the absence of the blending effect. We investigate the patterns of the DIA color-change curves for both single-lens and binary-lens events by constructing color-change maps.

Subject headings: gravitational lensing – stars: giants – limb darkening – photometry

1. Introduction

The amplification of source flux caused by gravitational lensing can become theoretically infinite. Points in the source plane at which the amplification of a point source becomes infinite are called caustics. For a point lens, the caustic is a single point behind the lens. For a binary lens, the number of caustics is multiple and they form closed curves. For a real microlensing event, however, the source star has an extended size, and thus the observed amplification deviates from that of a point-source event and becomes always finite:

extended source effect (Schneider, Ehlers, & Falco 1992; Witt & Mao 1994). The deviation of the light curve becomes most important when the source passes very close to the lens caustics.

Detection of the extended source effect is important because one can obtain useful information both about the lens and source star. First, a caustic-crossing event provides an opportunity to measure how long it takes for the caustics to transit the face of the source star. By using the source-radius crossing time t_*, along with an independent determination of the source star size θ_*, one can determine the lens proper motion with respect to the source star by $\mu = \theta_*/t_*$ (Witt & Mao 1994; Gould 1994; Maoz & Gould 1994; Nemiroff & Wickramasinghe 1994; Loeb & Sasselov 1995; Alcock et al. 1997b, 1997c, 1999a; Afonso et al. 1998; Udalski et al. 1998; Albrow et al. 1999a). Once the value of μ is determined, the mass and location of the lens can be significantly better determined. Second, by analyzing the light curve of an event in which source approaches very close to the caustics, one can determine the surface structure of the source star such as the surface intensity profile and spots (Valls-Gabaud 1994, 1998; Sasselov 1997; Gaudi & Gould 1999; Heyrovský & Sasselov 1999; Albrow et al. 1999b; Han, Park, & Jeong 1999).

The extended source effect can also be detected by measuring color changes during the event. The color changes occur due to the differential amplification over the limb-darkened source star surface (see § 3.1). Throughout this paper, we use a term "color-change curve" to refer to the color changes of an event induced by the extended source effect as a function of time. Detection of the extended source effect from the color measurements has the following advantages compared to the detection from a single band photometry. First, by detecting color changes one can increase the chance to detect the extended source effect. If the source star approaches very close to the caustics but does not transit the caustics, the amplification induced by the extended source effect simply masquerades as changes in lensing parameters, and thus cannot be detected. By contrast, the color change cannot be mimicked by the change in lensing parameters, because a point-source lensing event should be achromatic (Gould & Welch 1996). Second, by measuring the color changes one can determine the lens proper motion with relative ease. This is because one can measure t_*, and thus μ, of a caustic-crossing event by simply measuring the turning time of the color-change curve (Han, Park, & Jeong 1999, see § 4 for more details). To determine t_* from the light curve, on the other hand, it is required to fit the overall light curve.

However, precise measurements of the color changes induced by the extended source effect is hampered by the blending effect, which also causes color changes of an event (Kamionkowski 1995; Buchalter, Kamionkowski, & Rich 1996). To increase the event rate, the current lensing experiments are being conducted toward very dense star fields such as the Galactic bulge and the Magellanic Clouds (Alcock et al. 1993; Aubourg et al. 1993; Udalski et al. 1993; Alard & Guibert 1997). When the brightness of a source star located towards these very dense star fields is measured by using the current PSF photometry method, then, it is very likely that the measured source star flux is affected by the unwanted light from nearby unresolved stars (Di Stefano & Esin 1995; Alard 1997; Alcock et al. 1997a; Palanque-Delabrouille 1998; Woźniak & Paczyński 1997; Han 1999a; Han, Jeong,

& Kim 1998). Since the blended stars in general have different colors from the lensed source star color, the measured color is affected by the blending effect. Han, Park, & Jeong (1999) pointed out the seriousness of the blending effect in color-change measurements by demonstrating that even for a very small fraction of blended light, the color change caused by the blending effect can be equivalent to the color change induced by the extended source effect. Therefore, for the precise measurements of the color changes induced by the extended source effect, it will be essential to correct for or remove the blending effect.

Although numerous methods have been proposed for the correction of the blending effect (Alard, Mao, & Guibert 1995; Alard 1996; Han 1997, 1998, 1999b; Goldberg 1998; Goldberg & Woźniak 1998; Han & Kim 1999), most of these methods either have limited applicability only to several cases of blended events or are less practical due to the requirement of space observations.[1] On the other hand, with the recently developed photometric technique of the "difference image analysis" (DIA) method, one can measure the blending-free light variations of general microlensing events (Tomaney & Crotts 1996; Alard & Lupton 1998; Alard 1999; Alcock et al. 1999b, 1999c). However, due to the methodological difference of the DIA photometry from the conventional PSF photometry, the color change of an event measured by the using the DIA method (DIA color change) differs from that measured by the PSF method (PSF color change).

In this paper, we show that despite the difference in the measured color change from that measured by the PSF method, the DIA color-change curve of an event enables one to obtain the same information about the lens and source star, but with significantly reduced uncertainties due to the absence of the blending effect. We investigate the patterns of the DIA color-change curves for both single-lens and binary-lens events by constructing color-change maps.

2. Gravitational Amplification

2.1. Point-Source Events

If a gravitational microlensing event with a point source is caused by a single lens, the amplification of the event is represented by

$$A_{\rm p} = \frac{u^2+2}{u(u^2+4)^{1/2}}; \qquad u = \left[\left(\frac{t-t_0}{t_{\rm E}} \right)^2 + \beta^2 \right]^{1/2}, \tag{1}$$

where u represents the lens-source separation normalized by the angular Einstein ring radius $\theta_{\rm E}$ and the lensing parameters β, t_0, and $t_{\rm E}$ represent the impact parameter of the

[1]We note, however, that the MACHO group had *Hubble Space Telescope* followup observations of the source star for one of the events they have detected to clearly identify the lensed source star. From these observations, they could accurately estimate the lens mass by correcting the blending effect (NASA press release #STScI-PR00-03).

lens-source encounter, the time of maximum amplification, and the Einstein ring radius crossing time (Einstein time scale), respectively. The angular Einstein ring represents the effective region of gravitational amplification and its size is related to the physical parameters of the lens by

$$\theta_{\rm E} = \left(\frac{4GM}{c^2} \frac{D_{ls}}{D_{ol} D_{os}} \right)^{1/2}, \tag{2}$$

where M is the mass of the lens and D_{ol}, D_{ls}, and D_{os} represent the separations between the observer, the lens, and the source, respectively.

The amplification of a binary-lens event differs from that of a single-lens event. When lengths are normalized by the combined Einstein ring radius[2], the lens equation in complex notation for the binary-lens system is represented by

$$\zeta = z + \frac{m_1}{\bar{z}_1 - \bar{z}} + \frac{m_2}{\bar{z}_2 - \bar{z}}, \tag{3}$$

where m_1 and m_2 are the mass fractions of individual lenses (and thus $m_1 + m_2 = 1$), z_1 and z_2 are the positions of the lenses, $\zeta = \xi + i\eta$ and $z = x + iy$ are the positions of the source and images, and $\bar{z}$ denotes the complex conjugate of z (Witt 1990). The amplification of each image, $A_{{\rm p},i}$, is given by the Jacobian of the transformation (3) evaluated at the images position, i.e.

$$A_{{\rm p},i} = \left(\frac{1}{|{\rm det}\ J|} \right)_{z=z_i}; \qquad {\rm det}\ J = 1 - \frac{\partial\zeta}{\partial\bar{z}} \overline{\frac{\partial\zeta}{\partial\bar{z}}}. \tag{4}$$

Then the total amplification of the event is given by the sum of the individual amplifications, i.e. $A_{\rm p} = \sum_i A_{{\rm p},i}$. The binary-lens caustics are located at the source positions where ${\rm det}\ J = 0$.

2.2. Extended-Source Events

If the source of an event has an extended size, the light curve of the event deviates from that of a point-source event. For both single-lens and binary-lens events, the amplification of an extended source event is the weighted mean of the amplification factor over the source star disk, i.e.

$$A_\nu = \frac{\int_0^{r_*} I_\nu(r) A_{\rm p}(|\mathbf{r} - \mathbf{r}_L|) r dr}{\int_0^{r_*} I_\nu(r) r dr}, \tag{5}$$

where $I_\nu(r)$ is the radial surface intensity distribution of the source star with a radius r_* and the vector $\mathbf{r}_L$ and $\mathbf{r}$ represent the displacement vector of the source star center with respect to the lens and the orientation vector of a point on the source star surface with respect to the center of the source star, respectively.

[2]It represents the angular Einstein ring radius with a lens mass equal to the total mass of the binary system.

3. Color Changes

3.1. Measured by the PSF Method

In addition to causing deviations in the light curve from that of a point-source event, the exended source effect makes the gravitational amplification become wavelength dependent, causing color changes of the event. The color change occur due to the wavelength dependency of the source star radial surface intensity profile caused by limb darkening. If we define $F_{0,\nu i} = 2\pi \int_0^{r_*} I_{\nu i}(r) r dr; i = 1,\ 2$ and $m_{\nu i}$ as the unamplified source star fluxes and the corresponding magnitudes measured at two different wavelength passbands $\nu 1$ and $\nu 2$, the color of the un-blended source star measured at a time t by using the PSF method becomes

$$(m_{\nu 2} - m_{\nu 1})_{\rm PSF,0}(t) = -2.5 \log \left[\frac{A_{\nu 2}(t) F_{0,\nu 2}}{A_{\nu 1}(t) F_{0,\nu 1}} \right]. \tag{6}$$

Then the PSF color-change curve of an *un-blended* lensing events is represented by

$$\Delta(m_{\nu 2} - m_{\nu 1})_{\rm PSF,0}(t) = -2.5 \log \left\{ \left[\frac{A_{\nu 2}(t)}{A_{\nu 1}(t)} \right] \left[\frac{A_{\nu 2}(t_{\rm ref})}{A_{\nu 1}(t_{\rm ref})} \right]^{-1} \right\}, \tag{7}$$

where $t_{\rm ref}$ represents the reference time for the color-change measurements. For a point-source event, $A_{\nu 1}(t) = A_{\nu 2}(t)$ (i.e. achromatic), and thus $(m_{\nu 2} - m_{\nu 1})_{\rm PSF,0} = -2.5 \log(F_{0,\nu 2}/F_{0,\nu 1})$, implying that the color of the source during the event equals to that of the unamplified source and does not change. For a limb-darkened extended source event, on the other hand, as the caustics pass close to the source star, different parts of the source star disk with varying surface intensity and spectral energy distribution are amplified by different amount due to the differences in distance to the lens. As a result, the amplification becomes wavelength dependent, i.e. $A_{\nu 1}(t) \neq A_{\nu 2}(t)$, and the color changes during the event. Once the color-change curve of the event is constructed, the lens proper motion and the source star surface intensity profile are determined by statistically comparing the observed color-change curve to the theoretical curves with various models of limb darkening and source star size.

However, precisely measuring color changes induced by the extended sourece effect is hampered by the blending effect, which is another mechanism causing color changes. If one defines $B_{\nu i}$ as the blended amount of flux in two passbands, the measured color of a blended event becomes

$$(m_{\nu 2} - m_{\nu 1})_{\rm PSF}(t) = -2.5 \log \left[\frac{A_{\nu 2}(t) F_{0,\nu 2} + B_{\nu 2}}{A_{\nu 1}(t) F_{0,\nu 1} + B_{\nu 1}} \right] = -2.5 \log \left[\frac{A_{\nu 2}(t) + f_{\nu 2}}{A_{\nu 1}(t) + f_{\nu 1}} \right], \tag{8}$$

where $f_{\nu i} = B_{\nu i}/F_{0,\nu i}$ are the ratios between the blended flux and the baseline flux of the source star in the individual bands. Then the PSF color-change curve of a *blended* event is represented by

$$\Delta(m_{\nu 2} - m_{\nu 1})_{\rm PSF} = -2.5 \log \left\{ \left[\frac{A_{\nu 2}(t) + f_{\nu 2}}{A_{\nu 1}(t) + f_{\nu 1}} \right] \left[\frac{A_{\nu 2}(t_{\rm ref}) + f_{\nu 2}}{A_{\nu 1}(t_{\rm ref}) + f_{\nu 1}} \right]^{-1} \right\}. \tag{9}$$

One finds that equation (9) includes two additional blending parameters of $f_{\nu 1}$ and $f_{\nu 2}$ compared to the un-blended event curve in equation (7). Therefore, to determine the lens proper motion and the source star surface intensity profile from the fit of the blended event color-change curve, it is required to include these additional parameters. As a result, the determined quantities will suffer from increased uncertainties.

3.2. Measured by the DIA Method

The color changes induced by the extended source effect can also be measured by using the DIA method. The flux of a source star measured from the subtracted image by using the DIA method is

$$F_\nu = F_{\nu,\mathrm{obs}} - F_{\nu,\mathrm{ref}} = (A_\nu - 1)F_{\nu,0}, \tag{10}$$

where $F_{\nu,\mathrm{obs}} = A_\nu F_{0,\nu} + B_\nu$ and $F_{0,\mathrm{ref}} = F_{0,\nu} + B_\nu$ represent the source star fluxes measured from the images obtained during the progress of the event and from the reference image, respectively. Then the DIA color-change curve of an event is represented by

$$\Delta(m_{\nu 2} - m_{\nu 1})_{\mathrm{DIA}} = -2.5 \log \left\{ \left[\frac{A_{\nu 2}(t) - 1}{A_{\nu 1}(t) - 1} \right] \left[\frac{A_{\nu 2}(t_{\mathrm{ref}}) - 1}{A_{\nu 1}(t_{\mathrm{ref}}) - 1} \right]^{-1} \right\}. \tag{11}$$

From equation (11), one finds that the DIA color-change curve does not depends on the blending parameters, and thus it is free from the blending effect. One also finds that although the DIA color-change curve has a different form from that of the PSF curve of an un-blended event [cf. equation (7)], both curves depend on the same parameters of $A_{\nu 1}$ and $A_{\nu 2}$. Therefore, from the DIA color-change curve one can obtain the same information about the lens and source star as that obtained from the PSF color-change curve, but with significantly reduced uncertainties due to the absence of the blending effect.

4. Patterns of DIA Color-Change Curves

To see the patterns of DIA color-change curves, we construct color-change maps expected for both single-lens and binary-lens events. The constructed map are presented in the upper panel of Figure 1 (for the single-lens case) and Figure 2 (for the binary-lens case). To construct the maps, we assume that the source star has an angular radius of $\theta_* = 0.1\theta_{\mathrm{E}}$ and it is observed in U and I bands. The un-blended color of the source star before amplification is $(U - I)_{\mathrm{PSF},0} = 2.98$ mag, which corresponds to that of a K-type giant (Allen 1973; Schmidt-Kaler 1982; Peletier 1989). For the surface intensity profile, we adopt a linear form of

$$I_\nu(r) = 1 - \mathcal{C}_\nu \left[1 - \sqrt{1 - (r/r_*)^2} \right], \tag{12}$$

where the limb-darkening coefficients are $\mathcal{C}_U = 1.050$ and $\mathcal{C}_I = 0.053$, repectively, which correspond to those of a K giant with $T_{\mathrm{eff}} = 4,750$ K, $\log g = 2.0$, and a metallicity similar to the sun (Van Hamme 1993). For the binary-lens system, we adopt a binary separation of $\ell = 1.0\theta_{\rm E}$ and a mass ratio of $q = m_1/m_2 = 1.0$. The single-lens event map is presented as a function of lens positions (x_L, y_L) with respect the source star (the thick solid circle with its center at the origin), while the binary-lens event map is presented as a function of source position (ξ, η) with respect to the center of the binary system. All lengths in the maps are normalized by the angular Einstein ring radius. For both maps, we choose the reference of the color-change measurements to be $\Delta(U-I)_{\rm DIA} = 0$ when the source star is not gravitationally amplified. Grey scale is drawn so that it becomes brighter (darker) as the color of the source star becomes redder (bluer), and the tone of the grey scale changes for every color change of $\delta[\Delta(U-I)_{\rm DIA}] = 0.02$ mag. For the single-lens event map, the grey tone change from the darkest region where $\Delta(U-I) \leq -0.09$ mag to the brightest region where $\Delta(U-I) > 0.05$ mag. For the binary-lens event map, the tone changes from the darkest region where $\Delta(U-I) \leq -0.07$ mag to the brightest region where $\Delta(U-I) > 0.09$ mag. To better show the fine structures of the binary-lens event map in the region near the caustics (marked by thick solid curves), the region enclosed by a box (drawn by a short-dashed line) is expanded and presented in the upper panel of Figure 3. The straight lines in the upper panels of Figure 1 and Figure 3 represent various lens (for the single-lens case) or source (for the binary-lens case) trajectories and the color-change curves corrsponding to the individual trajectories are presented in the lower panel of the individual figures. The line types of the color-change curves are selected so that they match with those of the corresponding trajectories.

From the single-lens event color-change map and the resulting curves, one finds the following patterns. First, the iso-color-change contours are concentric circles with their center at the center of the source star. Due to the radial symmetry of the color-change map, all resulting color-change curves are symmetric with respect to the time of maximum amplification. Second, the color does not monotonically change as a function of the separation between the lens and the center of the source star, $r_L = \sqrt{x_L^2 + y_L^2}$. Outside the source star disk, the color of the event becomes redder as r_L decreases, but within the disk it becomes bluer with the decreasing value of r_L. As a result, while the color of a non-source-transit event continues to become redder as the lens approaches the source star, the color-change curve of a source-transit event is characterized by turns at the moments when the lens enters and leaves the source star surface. Measurement of the turning time, $t_\cap$, is important because one can determine the source-radius crossing time from the measured value of $t_\cap$ by

$$t_* = \left[\beta^2 + \left(\frac{|t_\cap - t_0|}{t_{\rm E}} \right)^2 \right]^{1/2} t_{\rm E}, \tag{13}$$

where the lensing parameters of β, t_0, and $t_{\rm E}$ are determined from the overall shape of the light curve. We note that the described patterns of the DIA color-change curves are very similar to those of the PSF color-change curves (see Han, Park,, & Jeong 1999).

The patterns of the binary-lens event color-change map and curves are as follows. First, compared to the single-lens event map, the map for the binary-lens events is much more complex. In the regions around fold caustics, the iso-color-change contours are parallel with the caustics, but the contours on the left and right sides of the caustics are not symmetric with respect to the caustic line. In the regions around cusps, on the other hand, the contours form separate peaks of blue color change. Second, the color-change curves are characterized by the turns during caustic crossings. The color becomes redder as the source approaches the lens caustics and becomes most reddish at around the time when the edge of the source star touches the caustics. By constrast, the color becomes most bluest when the inner region of the source star lies on the caustics. By measuring the time separation between the two red peaks, Δt, one can estimate the approximate value of the source-radius crossing time by

$$t_* \sim \frac{\Delta t}{2 \sin \phi}, \tag{14}$$

where ϕ is the angle at which the source crosses the caustics.[3] The value of ϕ can be determined from the global fit of the binary-lens event light curve.

5. Summary

In this paper, we investigate the chrometicity of single-lens and binary-lens microlensing events when their color changes are measured by using the recently developed DIA photometric method. The findings from this investigation are summarized as follows:

1. The DIA color-change curve of an event differs from the PSF curve of the same event.
2. Despite the difference, from the DIA color-change curve one can obtain the same information about the lens and source star as the information from the PSF color-change curve. This is because both the DIA and PSF color-change curves depend on the same parameters.
3. However, since the DIA color-change curve is not affected by the blending effect, one can determine the lens proper motion and source star surface intensity profile with significantly reduced uncertainties.
4. The DIA color-changes curves display various patterns depending on whether the event is caused by a single or binary lenses. Compared to the single-lens event curves, binary-lens curves are less symmetric and their patterns vary greatly depending on the lens system geometry.

---

[3]If the fold caustic is a straight line, the relation in equation (14) is exactly valid. However, for an extended source event the relation is an approximation because the fold caustics can no longer be treated a straight line.

5. The patterns of DIA color-change curves also vary depending on whether the source star transits the caustics or not. For caustic crossing events, one can measure t_* by measuring the turning time of the color-change curves.

This work was supported by the grant (KRF-99-041-D00442) of the Korea Research Foundation.

REFERENCES

Afonso, C., et al. 1998, A&A, 337, 17

Alard, C. 1996, in Proc. IAU Symp. 173, Astrophysical Applications of Gravitational Lensing, eds. Kochanek C. S. & Hewitt J. N., (Dordrecht: Kluwer), 215

Alard, C. 1997, A&A, 321, 424

Alard, C. 1999, A&A, 343, 10

Alard, C., & Guibert, J. 1997, A&A, 326, 1

Alard, C., & Lupton, R. H. 1998, ApJ, 503, 325

Alard, C., Mao, S., & Guibert, J. 1995, A&A, 300, L17

Albrow, M. D., et al. 1999a, ApJ, 512, 672

Albrow, M. D., et al. 1999b, ApJ, 522, 1011

Alcock, C., et al. 1993, Nature, 365, 621

Alcock, C., et al. 1997a, ApJ, 479, 119

Alcock, C., et al. 1997b, ApJ, 486, 697

Alcock, C., et al. 1997c, ApJ, 491, 436

Alcock, C., et al. 1999a, ApJ, 518, 44

Alcock, C., et al. 1999b, ApJ, 521, 602

Alcock, C., et al. 1999c, ApJS, 124, 171

Allen, C. W. 1973, Astrophysical Quantities, (London: Athlon Press), 208

Aubourg, E., et al. 1993, Nature, 365, 623

Buchalter, A., Kamionkowski, M., & Rich, R. M. 1996, ApJ, 469, 676

Di Stefano, R., & Esin, A. A. 1995, ApJ, 448, L1

Gaudi, B. S., & Gould, A. 1999, ApJ, 513, 619

Goldberg, D. M. 1998, ApJ, 489, 156

Goldberg, D. M., & Woźniak, P. R. 1998, Acta Astron., 48, 19

Gould, A. 1994, ApJ, 421, L71

Gould, A., & Welch, D. 1996, ApJ, 464, 212

Han, C. 1997, ApJ, 490, 51

Han, C. 1998, ApJ, 500, 569

Han, C. 1999a, MNRAS, 309, 373

Han, C. 1999b, ApJ, submitted

Han, C., & Kim, T.-W. 1999, MNRAS, 305, 795

Han, C., Jeong, Y., & Kim, H.-I. 1998, ApJ, 507, 102

Han, C., Park, S.-H., & Jeong, J.-H. 1999, MNRAS, submitted

Han, C., Kim, H.-I., Chang, K., & Park, S.-H. 1999, MNRAS, submitted

Heyrovský, D., & Sasselov, D. 1999, ApJ, submitted (astro-ph/9906024)

Kamionkowski, M. 1995, ApJ, 442, L9

Loeb, A., & Sasselov, D. 1995, ApJ, 449, L33

Maoz, D., & Gould, A. 1994, ApJ, 425, L67

Nemiroff, R. J., & Wickramasinghe, W. A. D. T. 1994, ApJ, 424, L21

Palanque-Delabrouille, N., et al. 1998, A&A, 332, 1

Peletier, R. F. 1989, Elliptical Galaxies: Structure and Stellar Content, PhD Thesis, (Groningen: Kapteyn Institute)

Sasselov, D. 1997, in Variable Stars and the Astrophysical Returns of Microlensing Surveys, eds. R. Ferlet, J.-B. Maillard, & B. Raban (Gif-sur-Yvette: Edition Frontières), 141

Schmidt-Kaler, Th. 1982, Landolt Bornstein: Numerical Data and Fundamental relationships in Science and Technology, eds. Schifers K. & Voigt H. H., (Berlin: Springer)

Schneider, P., Ehlers, J., & Falco, E. F. 1992, Gravitational Lenses (Berlin: Springer), 313

Tomaney, A. B., & Crotts, A. P. S. 1996, AJ, 112, 2872

Udalski, A., Szymański, M., Kalużny, J., Kubiak, M., Krzemiński, W., Mateo, M., Preston, G. W., & Paczyński, B. 1993, Acta Astron., 43, 289

Udalski, A., Kubiak, M., Szymanński, M., Pietrzýnski, G., Woźniak, P., & Żebruń, K. 1998, Acta Astron., 48, 431

Valls-Gabaud, D. 1994, in Large-Scale Structure of the Universe, eds. J. Mucket et al. (Singapore: World Scientific), 326

Valls-Gabaud, D. 1998, MNRAS, 294, 747

Van Hamme, W. 1993, AJ, 2096

Witt, H. 1990, A&A, 236, 311

Witt, H., & Mao, S. 1994, ApJ, 430, 505

Woźniak, P., & Paczyński, B. 1997, ApJ, 487, 55

This preprint was prepared with the AAS LaTeX macros v4.0.

Figure Captions

Figure 1: The single-lens event color-change map (upper panel) and crves (lower panel). The map is presented as a function of lens position (x_L, y_L) with respect to the source star (the thick solid circle). The source star has an angular radius of $\theta_* = 0.1\theta_{\rm E}$. The reference of the color change is chosen so that $\Delta(U-I)_{\rm DIA} = 0$ when the source star is not gravitationally amplified. Grey scale becomes brighter (darker) as the color of the source star becomes redder (bluer), and the tone of the grey scale changes with a color change interval of $\delta[\Delta(U-I)] = 0.02$ mag from the darkest region where $\Delta(U-I) \leq -0.09$ mag to the brightest region where $\Delta(U-I) > 0.05$. The lens trajectories (the straight lines in the upper panel) and their corresponding color-change curves are drawn by the same line types.

Figure 2: The binary-lens event color change map. The map is presented as a function of source star position (ξ, η) with respect to the positions of the binary lenses (marked by 'x'). The source star has an angular radius $\theta_* = 0.1\theta_{\rm E}$. The binary system has a separation between its components of $\ell = 1.0\theta_{\rm E}$ and a mass ratio of $q = 1.0$. The closed figure drawn by a thick solid curve represents the caustics of the binary-lens system. Grey scale is drawn by the same way as in Figure 1, but its tone changes from the darkest region where $\Delta(U-I) \leq -0.07$ mag to the brightest region where $\Delta(U-I) > 0.09$ mag. To better show the fine structures of the map in a region near the caustics, the region enclosed by a box is expanded and represented in the upper panel of Figure 3.

Figure 3: The binary-lens event color-change map (upper panel) near the caustic regions and the color-change curves (lower panel) resulting from various source star trajectories (straight lines). The region of the presented map corresponds to the enclosed part of the map in Figure 2. The grey tone of the map, the line types of the source trajectories, and the corresponding color-change curves are drawn by the same way as in Figure 2.

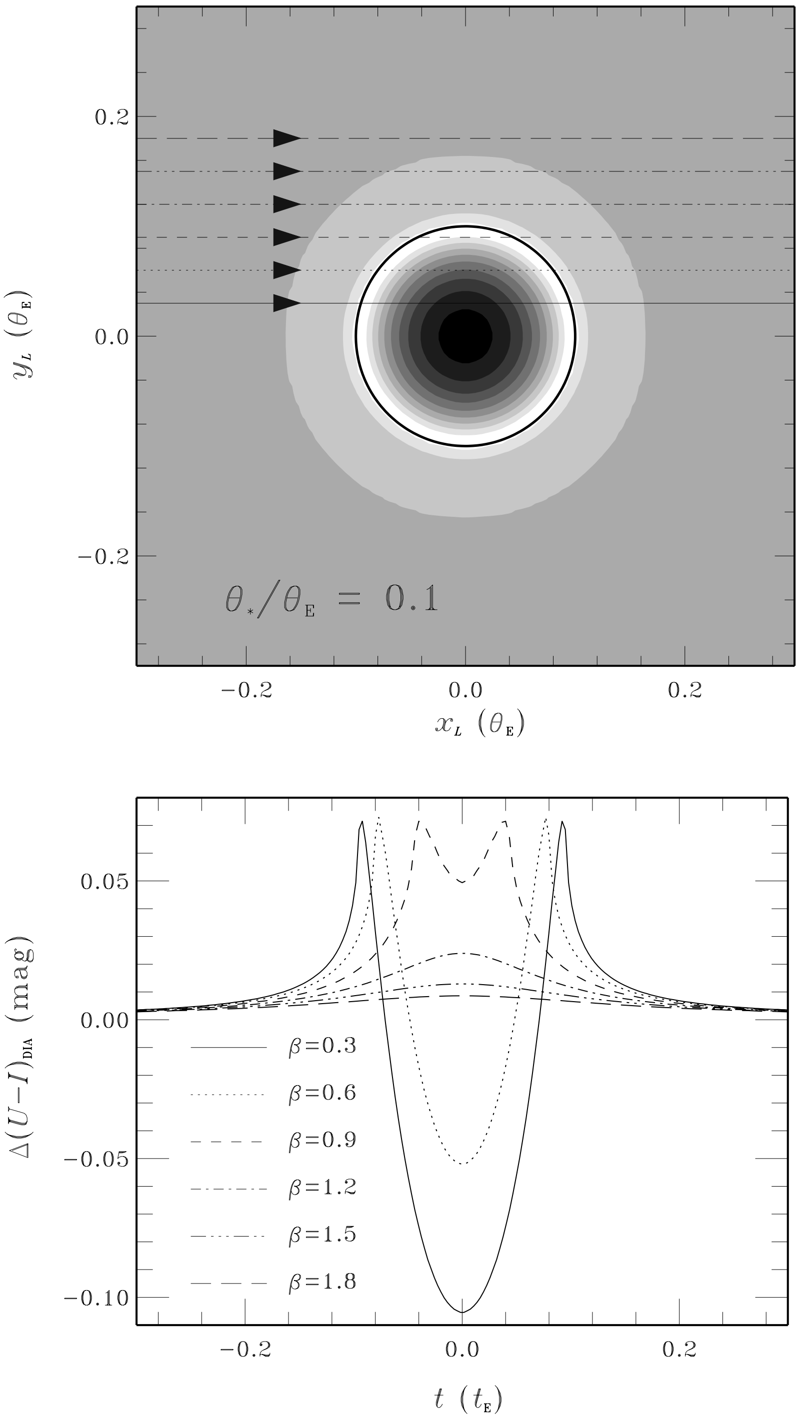
0.2
0.0
−0.2
y_L (θ_E)
θ_*/θ_E = 0.1
−0.2
0.0
0.2
x_L (θ_E)
0.05
0.00
−0.05
−0.10
$\Delta(U-I)_{DIA}$ (mag)
β=0.3
β=0.6
β=0.9
β=1.2
β=1.5
β=1.8
−0.2
0.0
0.2
t (t_E)

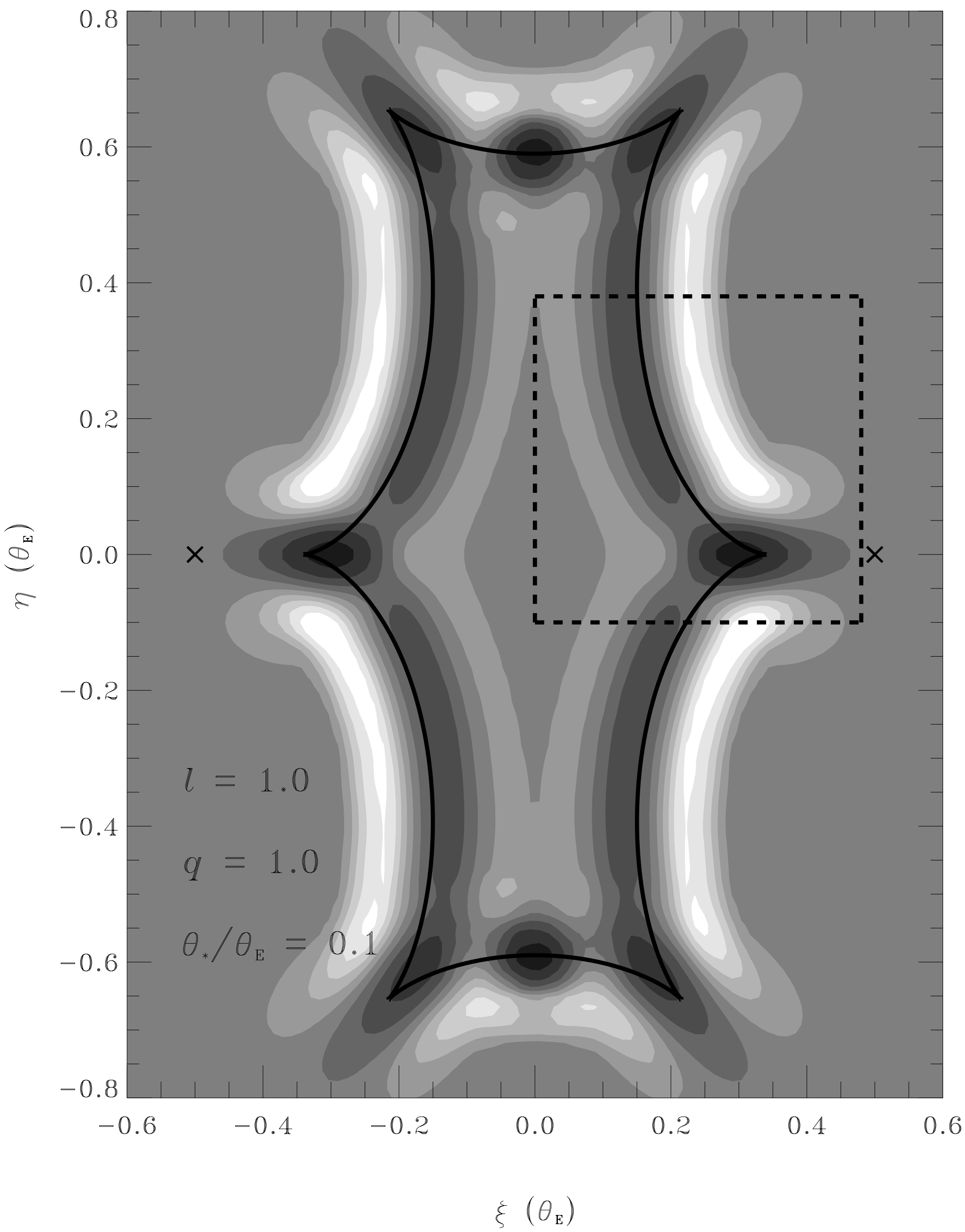

$l = 1.0$
$q = 1.0$
$\theta_*/\theta_E = 0.1$
$\eta\ (\theta_E)$
$\xi\ (\theta_E)$
0.8
0.6
0.4
0.2
0.0
−0.2
−0.4
−0.6
−0.8
−0.6
−0.4
−0.2
0.0
0.2
0.4
0.6

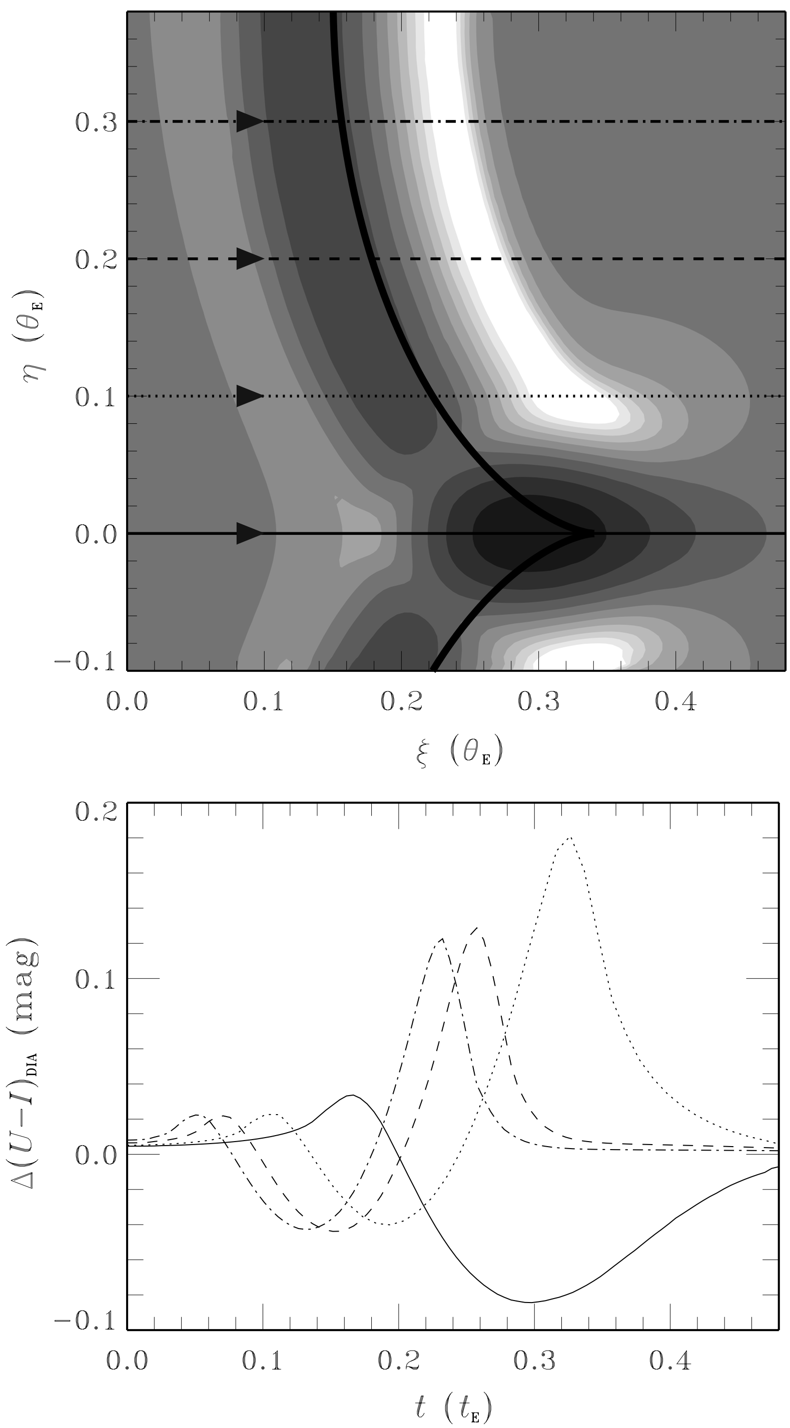

η (θ_E)
ξ (θ_E)
$\Delta(U-I)_{DIA}$ (mag)
t (t_E)